Microchannel Molding combined with Layer-by-Layer Approach for the Formation of three dimensional Tube-like Structures by Endothelial Cells

Bruno Aor[1,2,3,4], Irfan Khan[1,2,3,5], Karine Glinel[4], Alain M. Jonas[4], Sophie Demoustier-Champagne[4,*], Marie-Christine Durrieu[1,2,3,*].

[1]Univ. Bordeaux, Chimie et Biologie des Membranes et Nano-Objets (UMR5248 CBMN), Pessac (France)
[2]CNRS, CBMN UMR5248, Pessac (France)
[3]Bordeaux INP, CBMN UMR5248, Pessac (France)
[4]Institute of Condensed Matter and Nanosciences- Bio & Soft Matter, Université catholique de Louvain. Croix du Sud 1, box L7.04.02, 1348 Louvain-la-Neuve, Belgium
[5]Dr Panjwani Center for Molecular Medicine and Drug Research, University of Karachi, Karachi, Pakistan.
[*]Corresponding authors: sophie.demoustier@uclouvain.be, marie-christine.durrieu@inserm.fr

The development of a functional *in vitro* model for microcirculation is an unresolved challenge, with major impact for the creation and regeneration of organs in the tissue engineering. The absence of pre-vascularized engineered tissues limits enormously their efficacy and integration. Therefore, in this study, the i*n vitro* formation of tubular-like structures with human umbilical vein endothelial cells (HUVECs) is investigated thanks to three-dimensional polycarbonate (PC) micro-channel (µCh) scaffolds), surface biofunctionalized with hyaluronic acid/chitosan (HA/CHI) layer-by-layer (LbL) films grafted with adhesive (RGD) and angiogenic (SVV and QK) peptides, alone and in combination. The novelty of this work lies in the formation of capillaries in the order of tens µm, developing spontaneous micro-vessels, without the complexity of micro-fluidic approaches, and in a short time-scale. Ellipsometry, confocal laser scanning microscopy and fluorospectrometry are used to characterize the biofunctionalized micro-channels. PC-µCh scaffolds functionalized with $(HA/CHI)_{12.5}$ film (PC-LbL) and further grafted with RGD and QK peptides (PC-RGD+QK) or with RGD and SVV peptides (PC-RGD+SVV) are then tested for *in vitro* blood vessel formation. These assays evidence a rapid formation of tubular-like structures after 2h of incubation. Moreover, co-culture system involving HUVECs and human pericytes derived from placenta (hPCs-PL) stabilizes the tubes for longer time.

1. Introduction

The success of an engineered tissue often depends on the provision of an adequate blood supply to ensure efficient nutrition and oxygen supply [1]. This is possible by engineering a microcirculation system into three-dimensional constructs using, for example, an *in vitro* approach for this pre-vascularization step [1]. However, recapitulating the blood microcirculation in three-dimensional space is challenging for both engineered tissue grafts and model systems (such as organ-on-a-chip used to study angiogenesis in the presence of various drugs [2, 3]). The efficiency of a three-dimensional tissue construct can only be achieved when cells colonizing the graft can survive either *in vivo* for grafts or *in vitro* for tissue models. For both cases, oxygen delivery and perfusion, provision of nutrition, and waste removal need to match the metabolic demand [1, 4]. This is only possible when the degree of vascularization in the construct reflects the specific tissue requirement [1].

The vascularization of various grafts has already been tested *in vivo*, but only thin constructs or those requiring low metabolic demand such as skin, cartilage or bladder grafts have been successfully achieved and led to clinical translations [5, 6]. However, the vascularization challenge remains open for tissues highly sensitive to oxygen supply (*e.g.*, myocardium and liver).[2]. It is thus important to develop model systems which might induce a rapid vascularization in a stable and reproducible way, that would be potentially transferable to the fabrication of three-dimensional tissues.

Several approaches have been used both *in vivo* and *in vitro* [7-9] to create a scaffold containing a vasculature network that can be implanted in the patient and immediately integrated by the patient's body through anastomosis (*i.e.,* the connection between the scaffold and the patients' vascular network) [10, 11]. The successful development of a capillary network in a scaffold depends on four key factors: the cell lineage that is used to create the tubular structures, the template material which is both a mechanical support and a mechano-signal transductor, the extracellular matrix (ECM) which provides the proper micro-environment for cell culture, and finally supplementary factors such as peptides or growth factors which trigger specific signals inducing cell adhesion or angiogenesis [7, 8]. In addition, preserving the physiological size of a capillary vessel preserve their functionality and the bulk flow mechanism [12]. Oxygen exit from capillaries during the filtration step because the hydrostatic pressure is greater than the osmotic pressure thanks to the very small diameter of the capillaries in physiological conditions [13].

Compared to angiogenesis-inducing methods based on the delivery of growth factors or cell therapy, bioengineering approaches such as the use of sacrificial materials, 3D bioprinting and micropatterning [14] are advantageous because they can precisely control the geometry of the forming micro-vessels. In particular, the potential of using micro-channels as templates to guide *in vitro* the micro-vasculature by endothelial cells was already reported. [15-17]. However, the systems reported so far rely on large channels 40 to 200 µm in size, which considerably

differ from *in vivo* capillaries whose size is *ca.* 10-15 µm [18], and are therefore classified as giant capillaries [19, 20]. Here, we will focus on the development of tube-like structures by endothelial cells in smaller micro-channels, thereby more closely mimicking real capillaries.

Human umbilical vein endothelial cells (HUVECs) are widely used as optimal cell lineage candidates for the *in vitro* formation of capillary networks in engineered tissue grafts. Indeed, they preserve nearly all the native-vascular endothelium features found *in vivo* in physiological conditions [21]. In addition, HUVECs have been used in combination with other cell lines, peptides and other biological factors to mimic the *in vivo* conditions in which cells are surrounded by numerous soluble factors, extracellular matrix and supporting cells such as pericytes [11, 22, 23]. A detailed description of the cellular and molecular mechanisms of vascular lumen (tubular structure) formation was reported by Iruela-Arispe et al. [24]. Briefly, cord hollowing and cell hollowing are the two main mechanisms of lumen formation for endothelial cells. The first one involves at least two endothelial cells arranged in a paired fashion, which assemble into a cylindrical form, and coalescence vesicles creating the lumen [24, 25]. The second mechanism, cell hollowing, involves a single endothelial cell in which vacuoles are formed and coalesce inside the cell, creating an intracellular lumen [24, 25]. Both mechanisms require signaling from the ECM through cell-receptor binding involving vascular growth factor (VEGF) and osteopontin receptors, triggering intracellular signals to activate cdc42/Rac1 [24, 25].

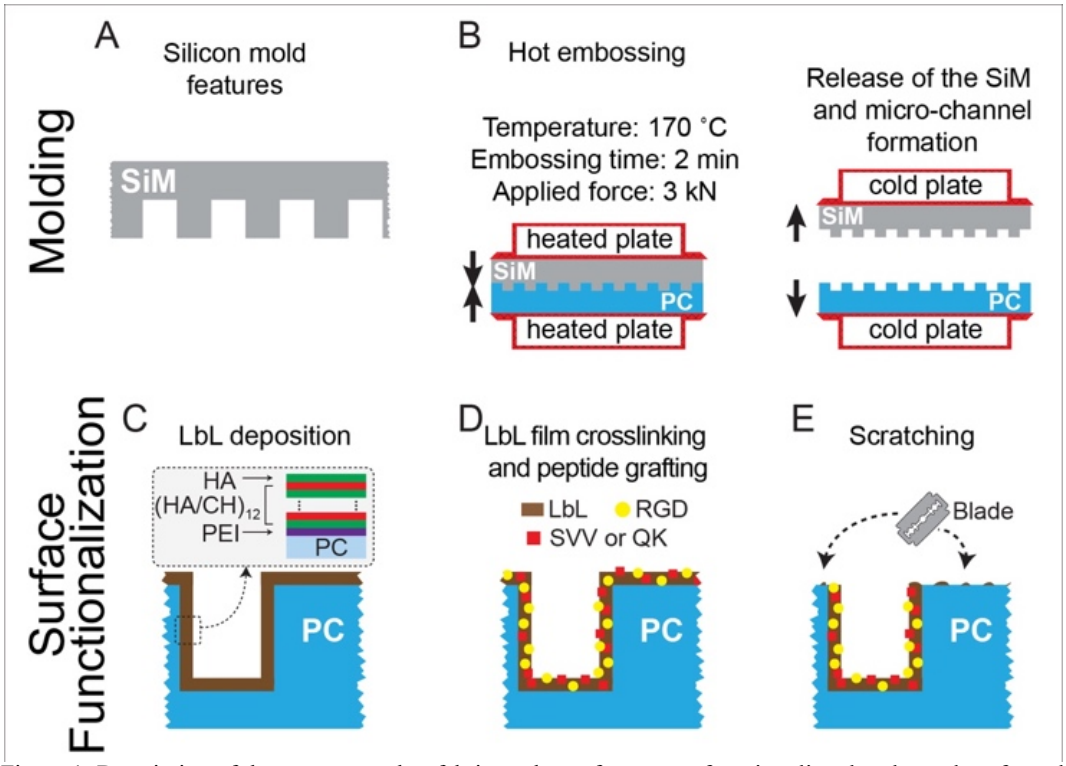

Figure 1: Description of the process used to fabricate the surface-modified PC microchannels (PC-µCh). (A) Scheme of the silicon mold (SiM) used to fabricate the PC-µCh. (B) Description of the hot-embossing process used to fabricate the PC-µCh. (C) Modification of the PC-µCh surface by LbL deposition of a PEI/(HA/CHI)12/HA coating. (D) Crosslinking of the LbL coating and grafting of different peptides (RGD, SVV, QK or a combination of those ones) through EDC/sulfo-NHS activation. (E) Selective removal of the bioactive coating on the top regions of the micropatterned PC sample by manual scratching.

This points to the need to properly biofunctionalize the surface of templating channels in order to allow cell adhesion and simultaneously trigger angiogenic pathways in endothelial cells. However, even though mimicking the geometrical and the chemical signals for endothelial cells might be sufficient to drive the formation of tube-like structures, it is unlikely to result in the formation of stable capillaries. Indeed, endothelial cells *in vivo* are constantly interacting with surrounding cells named pericytes, which contribute to stabilize the tubular structures [26]. A combination of two cell lines embedded in collagen was actually already shown to increase the lifetime of tube-like structures [27]. Therefore, the objective of the present study is to develop a simple model system for the rapid *in vitro* formation of stable capillary vessels by HUVECs, using a combination of geometrical and chemical cues, in the possible presence of pericytes. Nowadays in the literature most of the works lies in the formation of micro-vessels in the order of hundreds µm, or from pre-existing vascular network, or using complex microfluidic approach. Therefore the novelty of this work lies on the formation of micro-vessels in the physiological order of tens µm, guiding HUVECs to a spontaneous formation in a simple-and-reproducible manner with a rapidity never achieved before in the literature.

Briefly (Figure 1), we create micro-channels as small as 26 µm in a polycarbonate (PC) film by hot micro-embossing, then functionalize the channel surfaces by a crosslinked hyaluronic acid/chitosan layer *via* layer-by-layer (LbL) assembly [28]. This carboxylic acid-rich layer then serves to install peptides [28], either to improve adhesion (GRGDS a.k.a. RGD) [29] and/or to trigger angiogenesis a GDSVVYGLR (a.k.a. SVV) mimic of an osteopontin sequence [25, 30, 31], and/or a Ac-KLTWQELYQLK(Ac)YK(Ac)GI-amide (a.k.a. QK) mimic of

a VEGF sequence [32-34]. These functionalized channels stimulate HUVECs into forming tube-like structures, which we finally attempt to stabilize by co-culturing pericytes.

2. Materials and Methods

2.1. Materials

Polycarbonate films (PC) of 50 µm thickness were kindly provided by it4ip, Belgium. Polycarbonate pellets were purchased from General Electric (Lexan). Poly(ethyleneimine) (PEI) of 25 kg/mol molar mass was from Aldrich. Chitosan (CHI) of 50-150 kg/mol molar mass and a deacetylation degree higher than 90% (Protasan™ UP CL 114) was from NovaMatrix. Hyaluronic acid (HA) of 151-300 kg/mol molar mass was purchased from Lifecore Biomedical. N-(3-dimethylaminopropyl)-N'-ethyl-carbodiimide hydrochloride (EDC), N-hydroxysulfosuccinimide sodium salt (Sulfo-NHS), 4-(2-hydroxyethyl)piperazine-1-ethanesulfonic acid (HEPES), Fluorshield™ mounting medium with DAPI (DAPI), Cell Proliferation Kit II (XTT), poly(2-hydroxyethyl methacrylate) (poly-HEMA), rhodamine red, and toluidine blue were from Sigma-Aldrich. Sodium chloride (NaCl) were from Fisher Scientific. Fetal bovine serum (FBS), trypsin-EDTA, Quant-iT™ PicoGreen™ dsDNA Assay Kit, CellTracker™ Red CMTPX dye, CellTracker™ Green CMFDA dye, Alexa Fluor™ Phalloidin-546, Dulbecco's phosphate buffered saline (DPBS), and paraformaldehyde 16% (PFA) were purchased from Thermo Fisher Scientific. β-(N-morpholino)ethanesufonic acid (MES) was from ACROS. Ethanol (96 %), isopropanol (99.7%) and acetone (99.8%) were from VWR. Peptides with customized sequences were purchased from Genecust: GRGDS (RGD), GDSVVYGLR (SVV), Ac-KLTWQELYQLK(Ac)YK(Ac)GI-amide (QK), GRGDSK-fluorescein 5-isothiocyanate (RGD-FITC), GDSVVYGLRK-fluorescein 5-isothiocyanate (SVV-FITC), and Ac-KLTWQELYQLK(Ac)YK(Ac)GIK-fluorescein 5-isothiocyanate (QK-FITC). Human umbilical vein endothelial cells (HUVECs), human pericytes derived from placenta (hPCs-PL), endothelial basal medium 2 (EBM-2) with endothelial medium supplements, and pericytes growth medium (PGM) were purchased from Promocell. EGM-2 medium was prepared by adding the endothelial medium supplements to EBM-2. A silicon mold (SiM of 4 inches diameter) with a linear pattern was fabricated by combining photolithography and etching (WINFAB, UCLouvain), and later cut in 6 squares of 1 cm length. This mold was surface functionalized with 1*H*,1*H*,2*H*,2*H*-perfluorooctyl trichlorosilane [35]. MilliQ water was generated with a Millipore Sigma Simplicity Water Purification System.

2.2. Methods

Quick summary of the four methods involved can be found in the Supplementary file (Fig. S1 A,B,C,D).

2.2.1. Micro channel fabrication (Figure 1)

PC films were washed for 10 min with isopropanol then dried and shaped by a hot embossing procedure using a silicon master mold (SiM) composed of linear protrusions with a width of 25 µm, a height of 28 µm and an inter-distance between the protrusion edges of 25 µm (Fig. 1A). These obtained patterned PC films are named PC-µCh in the sequel. Molding was performed using a Fontijne hydraulic press (TP400, Fontijne Holland) as follows: the stacked PC film and SiM mold were sandwiched between two Kapton® sheets (260 µm thick), two silicone rubber sheets (about 1 mm thick) and two thick glass slides, then placed for 2 min between the plates of the press heated at 200˚C to pre-heat the stack (Fig. 1B). Then, a force of 3 kN was applied for 2 min, and the system was cooled down to 30˚C before releasing the pressure (Fig. 1B). PC-µCh were characterized by scanning electron microscope (SEM) and profilometry.

2.2.2. Bio-functionalization of PC substrates

PC substrates, i.e., either flat PC films or PC-µCh, were first modified with a LbL coating. For this purpose, HA, CHI and PEI polyelectrolytes were freshly dissolved at 1 mg/ml in 0.15 M NaCl, buffered at pH 6.0-6.5 and kept under stirring overnight at room temperature for a complete dissolution. Each deposition and rinsing steps were performed using a custom-made automatic dipping machine, holding the samples in a vertical orientation. Briefly, a PC substrate freshly cleaned with isopropanol was first dipped in the PEI solution for 10 min then rinsed three times in NaCl 0.15 M (pH 6.0) to create a positively charged surface. Afterwards, the PC sample was dipped alternatively in CHI and HA solutions for 5 min, each followed by three rinsing steps in NaCl 0.15 M (pH 6.0) solution (Fig. 1C). For further grafting of peptides, polysaccharides $(HA/CHI)_n$ architecture corresponding to the deposition of 12 (HA/CHI) bilayers plus one top HA layer were prepared. The multilayered films were then crosslinked by immersing the LbL-modified PC substrates into a freshly prepared EDC/sulfo-NHS solution (30 mM/50 mM in NaCl 0.15M, pH 5.0-5.5) overnight at 4˚C. After 16 h, the crosslinking reaction was stopped by performing eight washing steps of 20 min each in HEPES solution (20 mM in NaCl 0.15 M, pH 7.3-7.6).

Different peptides were covalently grafted on crosslinked PEI(HA/CHI)12.5 coatings deposited on PC substrates, denoted as PC-LbL. RGD, SVV, QK, RGD-FITC, SVV-FITC, and QK-FITC sequences were grafted alone or in combination through EDC/sulfo-NHS activation. The nomenclature of the peptide-modified samples will be PC-X in the sequel, with X being the name of the grafted peptide (or peptide combination). Briefly, a quick activation of the LbL multilayers with EDC/sulfo-NHS was performed for 15 min at RT, as described herein above, followed by one rinsing step in 0.1 M MES (pH 6.5). Then, the activated PC-LbL substrates were immersed into a peptide solution (10-4 M in 0.1 M MES buffer at pH 5.0-5.5) or peptide mixture (10-4 M RGD and 10-4 M SVV or QK in 0.1 M MES buffer at pH 5.0-5.5) overnight at 4˚C (Fig. 1 D, E). For the PC-µCh-XL samples, a further step of scratching with a metal blade was performed to remove the bioactive coating on the mesas between the channel grooves (Fig. 1 E). Finally, both flat PC-X and PC-µCh-X were washed eight times for 20 min each with 20 mM HEPES (pH 7.4 buffer followed by three rinsing steps of 5 min each in ethanol 50% then 30 min of sonication (30 Hz, 100W, Elmasonic P120H) in 50% ethanol to remove adsorbed peptide molecules.

2.2.3. Characterization of PC substrates before and after surface functionalization

2.2.3.1. Characterization of the silicon mold and micropatterned PC

Both SiM and PC-µCh samples were observed with a Field Emission Scanning Electron Microscope (FE-SEM) (JSM-7600F, Jeol Ltd.) operated at 15 keV to determine the protrusion or micro-channel width and inter-distance, respectively. Prior to their characterization by FE-SEM, all the PC-µCh samples were coated with a 10 nm-thick layer of Pt/Pd using a sputter coater (Cressington 208 HR). The height of the linear protrusions of the silicon mold and the depth of the microchannels of PC-µCh samples were measured by profilometry (Veeco Dektak 150) using the following settings: 'Hills and Valleys' profile mode, a scan duration of 100 s, a scan length of 100 µm, a stylus force of 4 mg, a stylus scan range of 524 µm and a stylus radius of 0.7 µm. At least three measurements were averaged per sample.

2.2.3.2. *Measurement of the LbL coating thickness*

The deposition of (HA/CHI) films on various surfaces has been extensively studied in the literature by various techniques such as atomic force microscopy, quartz crystal microbalance, zeta potential and FTIR [36-39].In our case, the growth of the films was investigated by ellipsometry. For that purpose, a PC solution (1g/L in dichloromethane) was spin-coated (Laurell WS-650MZ, speed 4500 rpm, acceleration 2250 rpm and time 60 s) on 1 cm2 silicon wafers to create a flat and homogeneous PC film with a thickness of about 6.1 ± 0.1 nm, followed by a single dipping step in a PEI solution to create an anchoring layer. Then, polysaccharide (HA/CHI)n films with different number (n) of deposited bilayers (n = 4, 8, 12, 16, 20, 24) were built and crosslinked on top of the PC-PEI film, using the procedure described hereinabove. The thickness of dried films was measured using a spectroscopic ellipsometer (Horiba-Jobin Yvon, France). The ellipsometry thickness was an average of four measurements, carried out at different spots on the surface of each sample.

2.2.3.3. *Quantification of free carboxylic groups available in the crosslinked LbL films*

Free carboxylic groups available in crosslinked PC-LbL samples for peptide grafting were quantified using toluidine blue-O (TBO) test, as previously reported [40, 41]. Briefly, 1 cm2 crosslinked PC-LbL samples were immersed in 5 mM TBO solution freshly prepared in NaOH 10 mM (pH 10). The reaction was carried out overnight then two quick rinsing steps in NaOH (pH 10) solution and Milli-Q water were performed. The samples were subsequently immersed in 5 mL acetic acid solution (50%) for 10 min to elute the TBO and the absorbance of the resulting solution was measured at 633 nm. The TBO concentration was evaluated using a calibration curve established from reference TBO solutions (with concentration varying from 10-4 to 10-8 M) (Fig. S2). We assumed that 1 mole of TBO was complexed with 1 mole of carboxylic acid groups to estimate the concentration of free carboxylic groups into the LbL films [42].

2.2.3.4. *Quantification of peptide grafting density*

In order to quantify the density of the different peptides grafted on/in the LbL films, samples grafted with fluorescent peptides (i.e., RGD-FITC, SVV-FITC and QK-FITC) were measured by fluorescence spectroscopy. Briefly, after biofunctionalization, disks of 6 mm in diameter were placed at the bottom of a black-96-well plate and 100 µL of DPBS 1X was added. PC films and PC-LbL samples not activated by EDC/sulfo-NHS were used as controls. The quantification of the grafted peptide was performed using a spectrofluorometer (CLARIOstar, λexcitation 488 nm, λemission 535 nm, gain 600, 30 x 30 matrix scan method). The amount of peptide grafted on each sample was evaluated from calibration curves plotted using reference FITC-peptide solutions with concentrations varying from 10-4 to 10-8 M (Fig. S3). Knowing the surface area of the analyzed sample, it was possible to determine the amount of peptide grafted on the LbL films (Table 1).

2.2.3.5. *Diffusion of peptides within the LbL multilayer*

To obtain more information about the ability of peptide molecules to diffuse within the crosslinked (CHI/HA) films, PC-X samples grafted with a FITC-peptide were imaged using an inverted confocal laser scanning microscopy (CLSM, ZEISS LSM 710). Briefly, flat PC-RGD-FITC samples were dipped in a rhodamine red solution (1 mM) for 5 min then quickly rinsed once with DPBS and placed upside-down onto a glass slide for CLSM analysis. Images of the sample were recorded at different Z positions in the green (RGD-FITC) and red (Rhodamine) channels, reaching the entire thickness of the sample. Afterwards, a Z-reconstruction of the film was performed (imageJ) to visualize the distribution of the two fluorophores within the film thickness.

2.2.3.6. *Characterization of the scratching of LbL film by fluorescence microscopy*

The bioactive coating present on the top mesas of the PC- µCh-LbL-RGD-FITC samples was removed by scratching the sample surface with a metal scalpel in the direction parallel to the channels. To visualize the efficiency of this approach, the scratching was performed only on half the surface of the sample. The different regions of the partially scratched sample were then imaged by fluorescence microscopy (LEICA). The images were acquired using a 10X objective and further analyzed with ImageJ (NIH, **http://rsb.info.nih.gov/ij/)** to measure the difference of fluorescence intensity between the scratched and unscratched regions, for both micro-channels and top mesas of the sample.

2.2.4. Characterization of PC substrates before and after surface functionalization

HUVECs were grown in a culture flask using EGM-2 supplemented with 20% FBS and supplement kit. Cells were sub-cultured using trypsin/EDTA and maintained at 37 °C in a humidified atmosphere containing 5% CO2. Cells at passages 4–6 were used for experiments.

hPCs-PL were grown in a culture flask using PGM supplemented with 20% FBS and supplement kit. Cells were sub-cultured using trypsin/EDTA and maintained at 37 °C in a humidified atmosphere containing 5% CO2. Cells at passages 4–6 were used for experiments.

2.2.4.1. *Metabolic activity test and DNA quantification*

An anti-cell-adhesive coating was deposited on 48-well plates (Costar, Corning) the day before the cellular experiments using a 3% poly-HEMA solution prepared in 96% ethanol according to the manufacturer's instructions (Sigma). Material sterilization was performed by immersion in 70 % ethanol for 15 min followed by a drying step for 45 min and three rinsing steps in DPBS 1X.

Metabolic activity tests were performed according to the manufacturer's (Roche) protocol on at least three replicates. Briefly, HUVECs were seeded (100 000 cells/cm2) on peptide-grafted samples placed in a non-adhesive 48-well plate, using EBM-2 medium. After 4 h incubation, the medium was replaced by EGM-2 supplemented with the XTT-Kit components (Roche). After an additional incubation of 4 h, the absorbance of the medium was measured with a microplate reader (ELx808 reader, BioTek) at two wavelengths 650 and 450 nm (Fig. S4 A). Similar control experiments were performed with cells on the tissue control plate (without material), with PC films, and with crosslinked PC-LbL samples incubated for 18 h (Fig. S4 A). DNA extraction was also performed on the same samples. For this, the samples were ultrasonicated for 10 s (Micro-tip, Misomx ultrasonic processor XL, Power 5) then PicoGreen Kit (Thermo Fisher Scientific) was used according to the manufacturer's instructions. Briefly, 10 µl of cellular lysate was collected and diluted 40 times with Component B of the XTT-Kit. Then 100 µl of this solution was transferred to a black-bottom 96-well plate (Eppendorf, France) and 100 µl of PicoGreen solution was added. The fluorescence signal of the resulting solution was measured at 520 nm with a microplate reader (CLARIOstar, France). Cell number was computed considering 6.6 pg of DNA per cell [43] (Fig. S4 B). The ratio between the measured absorbance from XTT test (Fig. S4 A) and the cell number obtained with PicoGreen method (Fig. S4 B) allowed us to compute what we define as corrected metabolic activity (Fig. 4).

2.2.4.2. HUVEC tube formation assays

48-well plates were coated with a poly-HEMA solution (0.1% in ethanol 98%) overnight. Then the well-plates were rinsed with sterile DPBS 1X and filled with PC-µCh-X samples that were disinfected for 15 min with ethanol (70%). 100 000 HUVECs/cm2 were resuspended in EBM-2 and seeded on the sample surface and the microplates were centrifuged at 900 rpm for 2 min to allow cells to align into the micro-channels. Then cells were cultured for various times (from 1 to 5h) and observed by CLSM after fixation. For this, a PFA solution (4% in DPBS 1X) was deposited on the sample surface. After an incubation time of 15 min, the surfaces were rinsed with DPBS, stained with Phalloidin-546 and mounted on a glass slide with FluorshieldTM DAPI for CLSM analysis (Leica DMi6000 Yokogawa). A total of 1062 images were acquired over 30 samples by using an oil objective 40X and by scanning the entire depth of the micro-channels. Afterwards, z-reconstructions were computed with ImageJ and the obtained images were analyzed with IMARIS 9.0 (Oxford Instruments, http://www.bitplane.com) for three-dimensional (3D) reconstruction of the confocal images and for analysis of the tubular structures of HUVECs into microchannels (n=3).

2.2.4.3. Co-culture assays for tube-stabilization

Co-culture experiments were performed using a protocol similar to the one described hereinabove for the tube formation. Briefly, 50 000 HUVECs/cm2 were firstly labeled with red cell tracker CMTPX and seeded on the material's surface. Two hours later, 50 000 hPCs-PL/cm2 were labeled with green cell tracker CMFDA and seeded on top of the HUVECs. Culture with only HUVECs was performed as negative control on tube-like structure stabilization. Samples and control were fixed after 2, 3, and 4 hours after HUVECs seeding, using the same procedure previously described. The experiments were performed twice, with 2 biological replicates per each condition for a total of 1188 images acquired with CLSM using an oil objective 40X and scanning the entire depth of the micro-channels. Z-reconstructions were computed with ImageJ to analyze the presence of tubular-like structures.

2.2.4.4. Statistics

Statistical analyses were performed using PRISM software (GraphPad Software, USA). Two way analysis of variance (ANOVA) was performed to compare sample means. When F values for a given variable were found to be significant, the Turkey correction test for multiple comparisons was used. Unpaired two-tailed student's t-test was performed to compare the mean of two samples which were considered following a Gaussian distribution. When F values for a given variable were found to be significant, the Welch's correction was used assuming different standard deviations. In both tests (two way ANOVA, and two-tailed student's t-test), results were considered to be significantly different starting from $p < 0.05$. The different p values are represented with different symbols in the graphs: $p < 0.05$ (*), $p < 0.01$ (**), $p < 0.001$ (***) and $p < 0.0001$ (****).

3. Results

3.1. Bio-functionalization of polycarbonate substrates

LbL films composed of chitosan (CHI) and hyaluronic acid (HA) (Fig. 2) were deposited onto PC substrates and crosslinked. Film build-up measured by ellipsometry after crosslinking reveals an exponential growth as expected for such a system [44] (Fig. 2). A dry thickness of about 110 nm was measured for a crosslinked PC-PEI/(HA/CHI)12.5 sample (i.e., PC-LbL) used in the sequel.

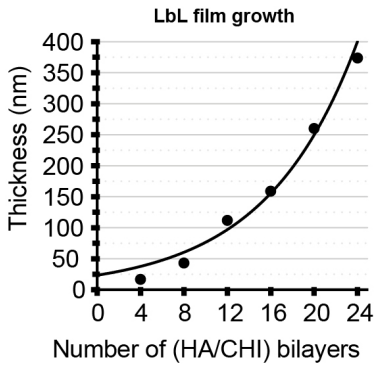

Figure 2: Growth of (HA/CHI) crosslinked LbL films deposited onto a PEI-modified PC surface and measured by ellipsometry in the dry state.

Prior to the immobilization of adhesive and angiogenic peptides on crosslinked PC-LbL samples, the amount of remaining available carboxylic groups on these samples was determined using toluidine blue (TBO) test. A high COOH group density of 73 ± 4 pmol/mm2, corresponding to 43 COOH groups/nm2, was obtained. These COOH groups are located over the whole thickness of the LbL which explains the high value of measured COOH group density. In order to optimize the peptide grafting process onto the LbL coating, preliminary grafting tests using a fluorescently tagged peptide, RGD-FITC (Fig. 3 B) were performed. RGD-FITC was immobilized on different PC-based substrates and under different grafting conditions: bare PC film exposed to the peptide without EDC/sulfo-NHS, PC coated with a crosslinked PEI/(HA/CHI)12.5 LbL film then exposed to the peptide without EDC/sulfo-NHS activation (samples named PC-LbL) and PC coated with a crosslinked PEI/(HA/CHI)12.5 LbL film then exposed to the peptide with EDC/sulfo-NHS activation (samples named PC-RGD). To remove the unreacted peptide at the end of the grafting procedure, the different samples were submitted to a sonication step of varying duration. The amounts of peptide detected on the surface without any sonication step and after 30 or 60 min of sonication were quantified by fluorescence spectroscopy and are reported in Fig. 3A.

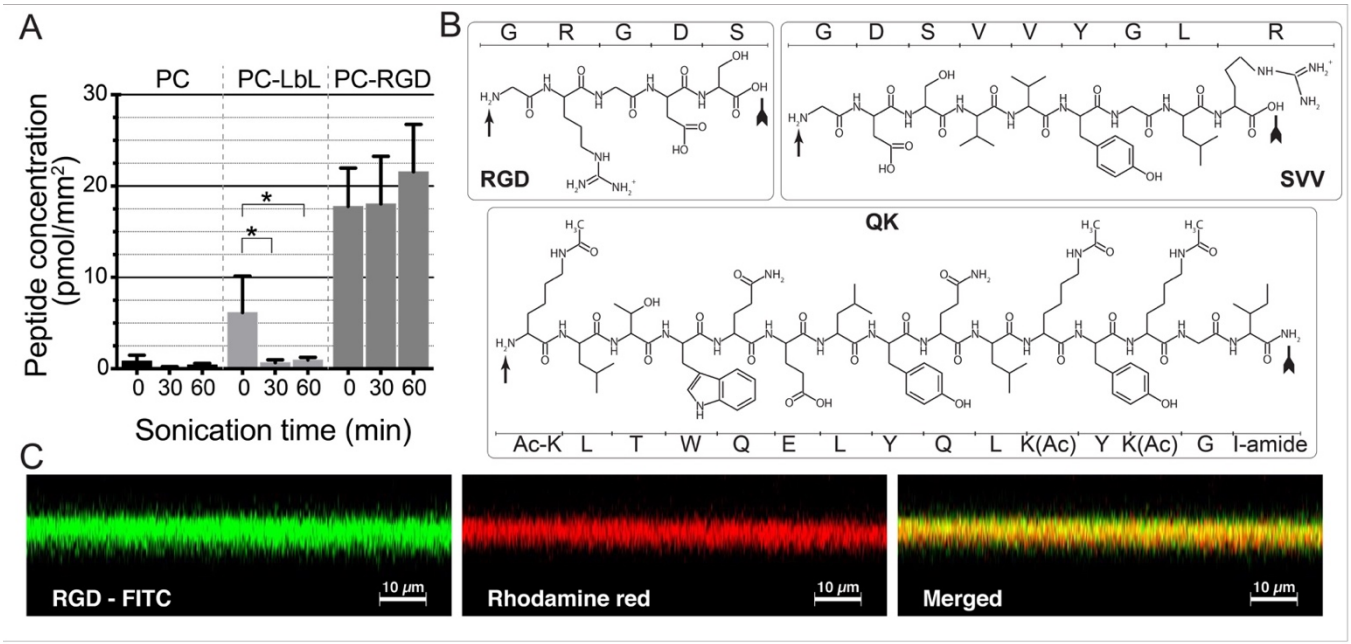

Figure 3: Characterization of PC substrates modified with various peptides. (A) Quantification of the amount of RGD-FITC peptide immobilized onto bare PC, PC coated with a crosslinked PEI/(HA/CHI)12.5 LbL film then exposed to the peptide without EDC/sulfo-NHS activation (PC-LbL) and PC coated with a crosslinked PEI/(HA/CHI)12.5 LbL film then exposed to the peptide with EDC/sulfo-NHS activation (PC-RGD). The amount of immobilized peptide is measured by fluorescence spectroscopy after a sonication period of 0, 30 or 60 min to remove the unreacted peptide. (B) Chemical structure of the different peptides grafted on PC substrates. Black arrows indicate the amine group used to immobilize the peptide onto the surface through the EDC/sulfo-NHS activation; arrow tails indicate the functional group grafted with a fluorescent dye. (C) Z-reconstructions computed from CLSM images recorded for a PC substrate coated with a PEI/(HA/CHI)12.5 film then grafted with RGD-FITC peptide (PC-RGD) and labeled with rhodamine red: reconstruction computed from green (left) and red channel images (middle) and overlay images (right). The CLSM images were recorded in liquid. The scale bar is the same in all directions.

On bare PC films, the measured amount of peptide was 0.9 ± 0.3, 0.1 ± 0.05 and 0.4 ± 0.1 pmol/mm2, after a sonication step of 0, 30 or 60 min, respectively. The statistical analysis revealed no significant differences between these three samples (Fig. 3A). On PC-LbL samples, the evaluated adsorbed peptide amount was 7 ± 2 pmol/mm2 (without any sonication step), while after 30 and 60 min sonication time, this value fell down to 0.7 ± 0.1 and 0.9 ± 0.1 pmol/mm2, respectively. In this case, the statistical analysis identified a significant difference between the value obtained at 0 min of sonication and both other values measured after 30 and 60 min of sonication (Fig. 3A). Finally, on PC-RGD samples, the measured amount of immobilized peptide, without any sonication, was equal to 18 ± 3 pmol/mm2 and remained stable at values around 18 ± 2 and 21 ± 2 pmol/mm2, after a sonication step of 30 and 60 min, respectively. The statistical analysis revealed no significant differences between these three values for the PC-RGD samples (Fig. 3A). Therefore, 30 min of sonication was used as standard protocol for all further peptide grafting experiments.

The density of immobilized peptide was quantified for the three different peptides using the corresponding calibration curve (Fig. S3). The density values are reported in Table 1 in different units to further facilitate the comparison with the literature in the discussion section. The lowest grafted peptide density, 18 pmol/mm2, was obtained for RGD peptide (PC-RGD), followed by SVV (PC-SVV) which results in an intermediate density of ca. 34 pmol/mm2. The highest peptide grafting density, 55 pmol/mm2, was observed for QK immobilization.

Table 1: Peptide densities (mean ± standard error) determined by fluorescence spectroscopy for PC-RGD, PC-SVV and PC-QK.

	Density of the grafted peptide	
	Mean ± standard error	Mean ± standard error
Sample	pmol/cm²	molecules/nm²
PC-RGD	1800 ± 310	11 ± 2
PC-SVV	3400 ± 370	20 ± 2
PC-QK	5500 ± 150	33 ± 1

Two tests were performed in order to determine if the peptides are only grafted on the top surface of the LbL films, present a gradient of concentration in the film thickness or are homogenously distributed within the film. First, the penetration depth of RGD-FITC after immobilization on PC-LbL was measured (Fig. 3C, left) in 0.15 M NaCl at pH 6.0 using CLSM. Then, the overall LbL layer thickness was determined by labeling the LbL film with rhodamine (Fig. 3C, middle) in the same conditions. It was found that the penetration depth of the RGD peptide was overlapping with the signal of the LbL layer thickness (Fig. 3C, right), resulting in a penetration depth equal to the hydrated film thickness (6 ± 1 µm).

3.2. Measurement of HUVECs metabolic activity

Prior to tubulogenesis experiments within bio-functionalized PC-µCh, the impact of the material's surface biochemistry on HUVECs adhesion and metabolic activity was investigated on various flat PC films. For that purpose, HUVECs were seeded on PC-LbL, PC-LbL grafted with a single peptide (RGD, SVV or QK) and on PC-LbL grafted with a combination of two peptides, either RGD + SVV or RGD + QQ. Metabolic activity (XTT) and cell number (PicoGreen) tests were then performed after 18 h culture on all these samples. Results obtained from XTT (Fig. S4 A) and PicoGreen (Fig. S4 B) tests allowed to compute the corrected metabolic activity, which is expressed as the ratio between the measured absorbance and the cell number (Fig. 4). As shown on Figure 4, the corrected metabolic activity measured on PC-RGD samples is significantly higher than the metabolic activity measured on PC-SVV and PC-QK samples, confirming a higher activity of cells grown on PC-LbL films grafted with RGD peptide. But, an even higher metabolic activity is observed when a combination of two peptides, either RGD + SVV or RGD + QK, are grafted onto the surface of PC-LbL samples.

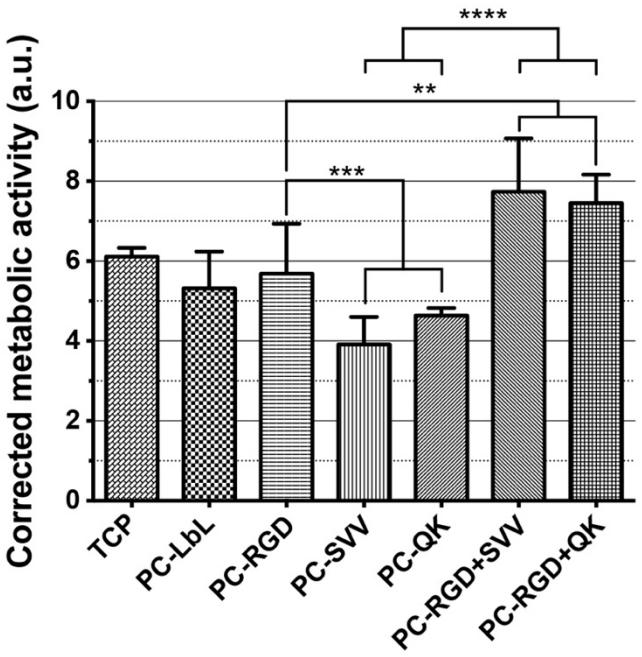

Figure 4: The metabolic activity corrected by the cell number measured for HUVECs cultured for 18 h on different flat surfaces. p value < 0.001 (***) when comparing PC-SVV and PC-QK samples, p value < 0.01 (**) when comparing PC-RGD+SVV and PC-RGD+QK, p value < 0.0001 (****) when comparing PC-SVV and PC-QK with PC-RGD+SVV and PC-RGD-QK samples.

3.3. Micro-channel characterization

Three-dimensional micro-channels were fabricated from PC films by hot embossing. A line grating silicon master mold (SiM) with linear protrusions of defined width (w), spacing (s) and height (d) (Fig. 5A) was characterized by SEM and profilometry (Fig. 5C and 5E). The values measured for the linear protrusion width and spacing was 25.13 ± 0.03 µm (white arrow) and 24.47 ± 0.04 µm (black arrow), respectively. The average height of the linear protrusions was 26.19 ± 0.01 µm (n = 25). The same characterizations were performed on the molded PC films (Fig. 5B) which present microchannels with a width (w') of 26.09 ± 0.07 µm (white arrows), a spacing (s') of 22.40 ± 0.07 µm (black arrow) and a depth (d') of 25.74 ± 0.05 µm (n = 25) (Fig. 5D and 5E). Therefore, the dimensions of the microchannels are in a good agreement with the geometrical characteristics of the mold. The dimensional differences are likely being due to differences of electron emission between the conduction Si master and the insulating polymer film, resulting in different definitions for the location of edges.

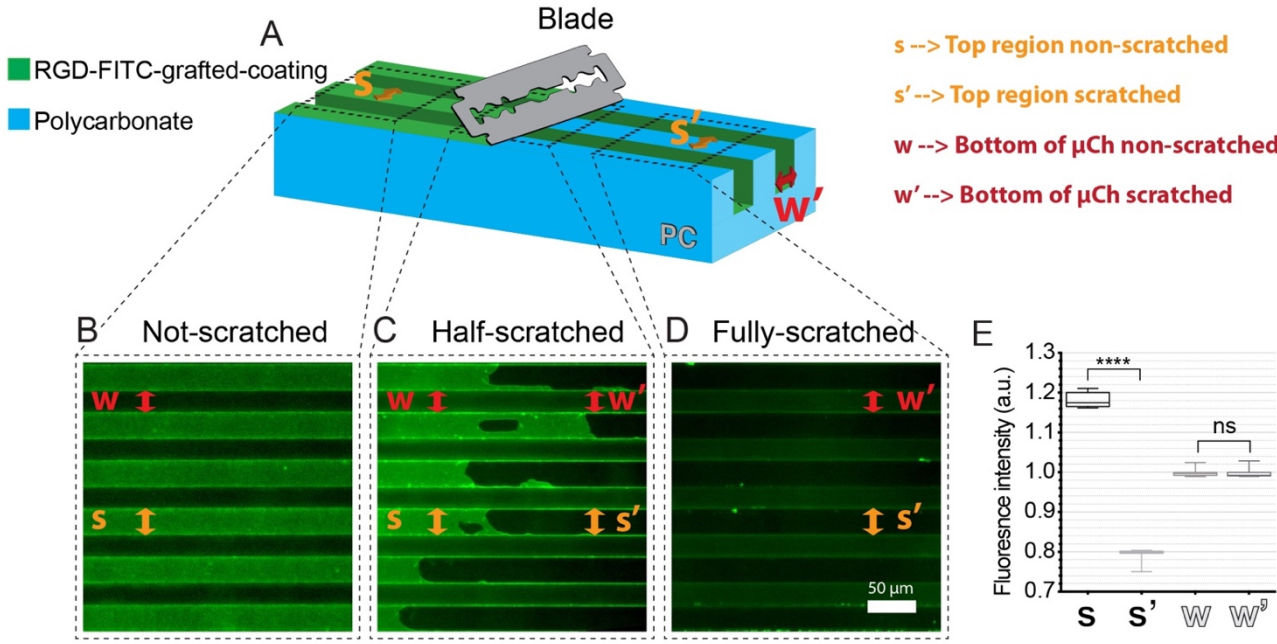

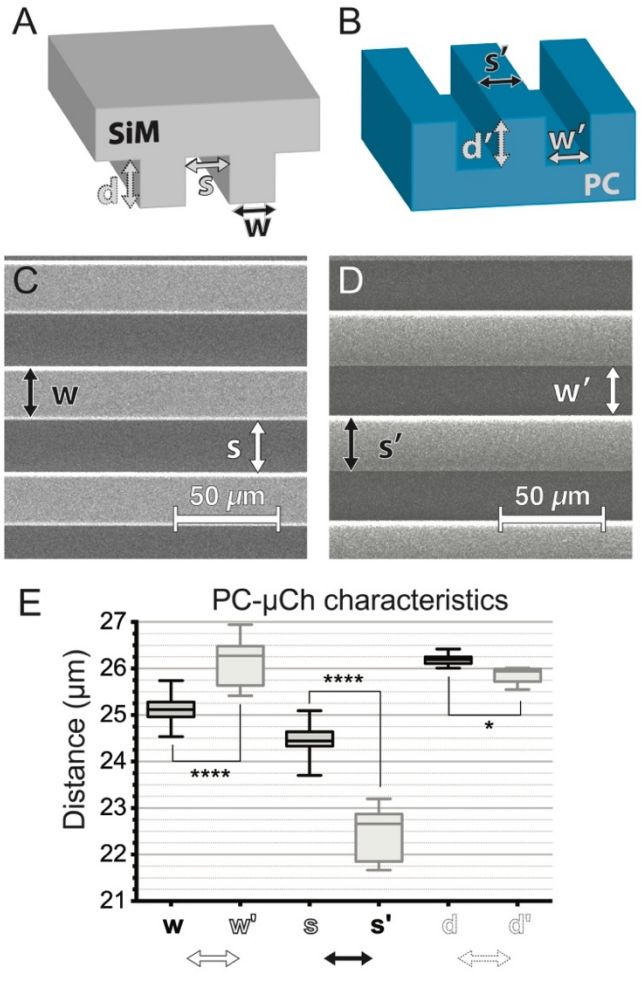

Figure 5: Characteristics of PC-µCh. (A) Schematic representation of the silicon mold (SiM) used to prepare the PC-µCh: distance between two linear protrusions (s), width (w) and height (d) of the linear protrusions. (B) Schematic representation of PC-µCh: distance between two channels, width (w') and depth (d') of the channels. Top view SEM images of the silicon mold (C) and PC-µCh (D). Small letters are described in (A) and (B). (E) Geometrical characteristics of SiM and PC-µCh measured by SEM and profilometry.

PC-µCh samples were then functionalized with cross-linked PEI/(HA/CHI)12.5 LbL films and grafted with peptides according to the protocol used to functionalize flat PC films. To obtain micropatterned PC samples showing bioactive surface only inside the micro-channels, the top surface of the biofunctionalized PC-µCh samples was mechanically scratched with a metal blade after functionalization. In order to check the efficiency of this procedure, a scratch test was performed on half the surface of a PC-µCh sample modified with a LbL-RGD-FITC coating, as schematized in Fig. 6A. Fluorescence images were then recorded from three different regions of the sample (Fig. 6B, 6C, 6D and 6E). The comparison of the fluorescence intensity values extracted from these images reveals a statistically-significant decrease between the mesas located in the unscratched (s) and scratched (s') regions (Fig. 6E). By contrast, no significant difference was observed between the intensity signal measured into the microchannels located in the scratched (w') and unscratched (w) regions (Fig. 6 E).

Figure 6: Characterization of the mechanical scratching performed on surface-modified PC-µCh to remove the coating from the top mesas of the sample. (A) Schematic representation of the scratching process. Fluorescence images recorded in the unscratched (B), partially scratched (C) and scratched regions (D) of a PC-µCh sample which is surface-modified with a crosslinked LbL film grafted with RGD-FITC. (E) Measurements of the fluorescence intensity in the different regions of the scratched sample (see (A) for the description of the different regions of the sample). p value < 0.0001 (****) between s and s'.

3.4. HUVEC tube formation in microchannels

CLSM measurements were performed on HUVECs cultured for various times on different samples to observe the possible

formation of tubular structures. PC-μCh-RGD+QK and PC-μCh-RGD+SVV were selected because of the presence of the adhesive peptide (RGD) and one angiogenic peptide (either SVV or QK), and PC-μCh-LbL without any grafted peptide was selected as negative control (Fig. 7). After an incubation time of 1 h, HUVECs cultured on PC-μCh-RGD+QK samples just started the adhesion process inside the microchannels as can be seen by the inspection of their morphology which is mostly round-shape but with the presence of adhesion sites (Fig. 7A, T-1h). In addition, cells are exclusively localized inside the channels, preferentially on the bottom of the channels. After 2 h, HUVECs are able to migrate from the bottom of the channels to their sides to form a tubular structure (Fig. 7A, T-2h white arrow and dashed line). After 3 h, HUVECs maintain their typical tube-like structure (Fig. 7A, T-3h white arrow) but also start to migrate to the top mesas of the sample located between the channels (Fig. 7A, T-3h). After 4 h, the tube-like structure is still maintained (Fig. 7A, T-4h) with more HUVECs migrating on the top mesas (Fig. 7A, T4h). After 5 h, all the HUVECs show the same morphology spreading both inside and outside the micro-channels, without the presence of tubular structure (Fig. 7A, T5h).

On the PC-μCh-RGD+SVV samples, after 1 h incubation, cells just started the adhesion process, mostly inside the microchannels, as seen for PC-μCh-RGD+QK samples (Fig. 7B, T-1h). After 2 h, HUVECs show the same tubular structure as the one observed on PC-μCH-RGD+QK sample (Fig. 7B, T-2h white arrow). After 3 h, HUVECs lose their capability to maintain the tubular structure and adhere on the entire surface of the microchannels (Fig. 7B, T-3h white arrow) with limited migration to the top mesas of the sample. After 4 h, HUVECs spread outside the channels, migrating from the channels to the top mesas of the sample (Fig. 7B, T-4h). After 5 h, all the HUVECs show an indiscriminate growth both inside and outside the channels, without the presence of tubular structure (Fig. 7B, T-5h).

On the PC-μCh-LbL sample, the formation of the tubular structure is completely absent after all the incubation times tested (Fig. 7C). In all the time points analyzed, HUVECs preserve their round-shape morphology, showing their very poor capability of adhesion or migration on the microchannel surface (Fig. 7C, T1h-T5h). Even at the last time point, HUVECs do not migrate to the top mesas of the sample, as observed for the two other samples.

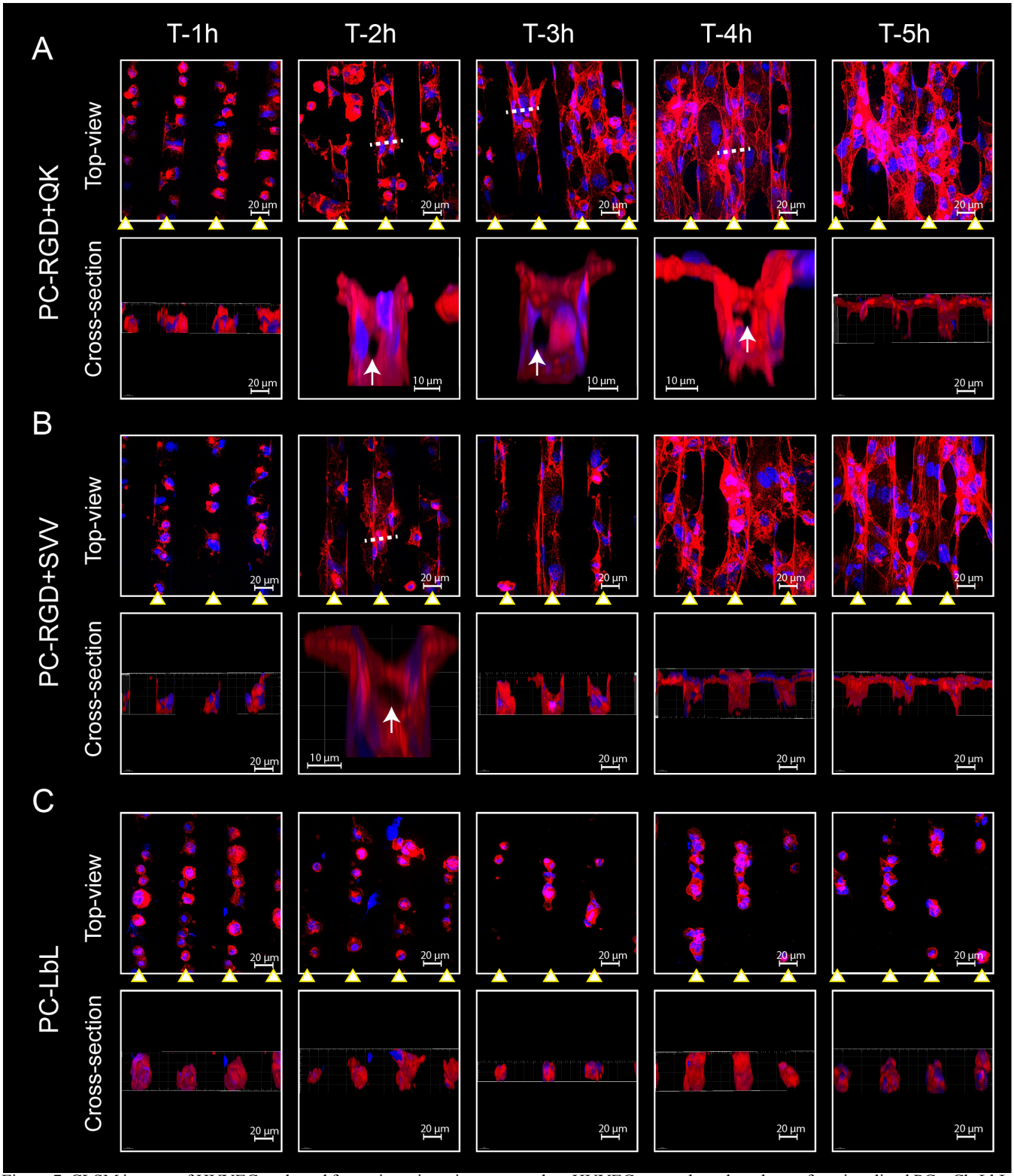

Figure 7: CLSM images of HUVECs cultured for various times into microchannels of PC-µCh samples surface-modified with crosslinked LbL (C, PC-µCh-LbL), crosslinked LbL grafted with RGD+QK (A, PC-µCh-RGD+QK) and crosslinked LbL grafted with RGD+SVV (B, PC-µCh-RGD+SVV). (A) Cells cultured on the PC-µCh-RGD+QK sample lead to the formation of a tubular-like structure with a lumen between 2 and to 4h incubation (white arrows). (B) The PC-µCh-RGD+SVV sample leads to the formation of a similar structure but only after 2h incubation (white arrows). (C) No formation of tubular-like structure is observed when HUVECs are cultured on the no-functionalized PC-µCh-LbL sample. Cell nuclei and cytoskeleton are stained with DAPI (blue) and Phalloidin-546 (red). The yellow arrows shown in the top view images indicate the locations of the microchannels, which run vertically in the top-view images.

3.5. *Tube-like structure stabilization*

Co-culture of HUVECs and hPCs-PL was performed for various times on the PC-µCh-RGD+SVV samples, for which HUVECs alone were not capable to sustain a tube-like structure for more than 2 hours. CLSM observations were performed on PC-µCh-RGD+SVV, after cell fixation, to evaluate the formation and stabilization of tube-like structures after 2, 3, and 4 hours (Fig. 8). In this experiment, we focused our attention on the observation of cells located inside the microchannels and we analyzed the cross-section of each image to study the variation of the tube-like structure. After 2 h of mono-culture with HUVECs, the formation of a tube-like structure with a lumen component was observed (Fig. 8A, dashed circle). However, when this culture was continued for longer time, the lumen disappeared (Fig. 8 B, D). However, when hPCs-PL are introduced in the culture, the lumen structure was preserved after 3 and 4 h of incubation (Fig. 8 C, E, dashed closed curves).

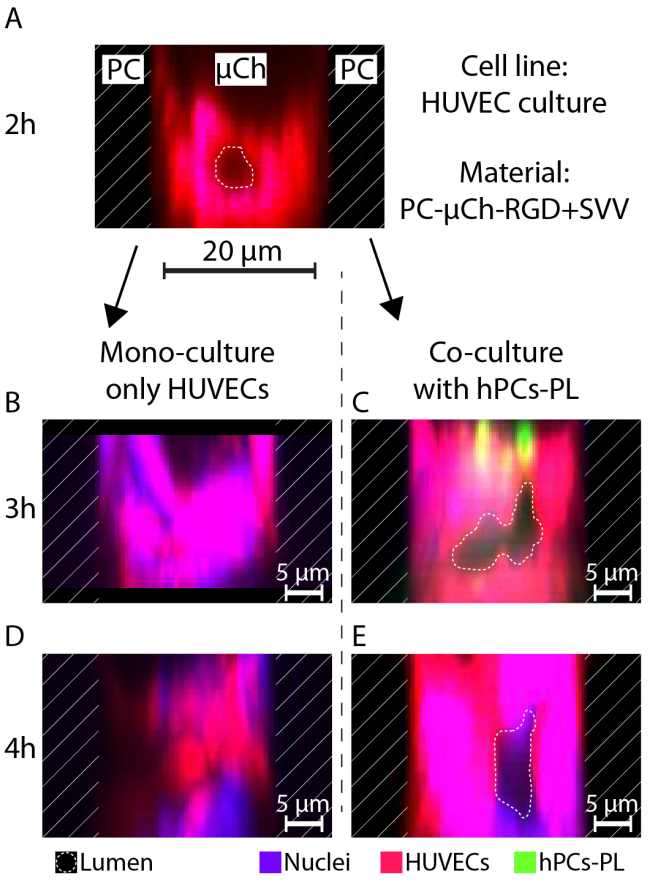

Figure 8: CLSM images showing the stabilization of tube-like structures by co-culturing HUVECs and hPCs-PL on PC-µCh-RGD+SVV samples. Mono-culture of HUVECs performed for 2h (A), 3h (B) and 4h (D) indicate the formation of the lumen (dashed circle) after 2h and its disappearance after 3h. Co-culture of HUVECS and hPCs-PL stabilizes the lumen developed by HUVECs after 2 h since the lumen is still observed after 3 h (C) and 4 h culture (E). Cell nuclei are stained with DAPI (blue), HUVECs cytoplasm with CMTPX (red) and hPCs-PL cytoplasm with CMFDA (green).

4. Discussion

In the present work, we successfully developed a model system combining three-dimensional geometrical cues with material surface functionalization to guide HUVECs in developing capillary-like tubular structures. The followed strategy includes three main steps. First, molding of PC films to generate microchannels of well-controlled depth, spacing and width (PC-µCh). Second, bio-functionalization of the PC surface with charged polysaccharides using the versatile LbL deposition process [45], and further grafting of different adhesive or angiogenic peptides. Third, culture of HUVECs and hPCs-PL on these bioactive micropatterned surfaces to evaluate the impact of the surface chemistry of the micropatterned substrates on the metabolic activity of cells and their capability to form a stable tubular-like structure. Different types of samples were tested: PC-µCh-RGD, PC-µCh-SVV, PC-µCh-QK, PC-µCh-RGD+SVV and PC-µCh-RGD+QK

Hot embossing appears to be an easy and highly reproducible procedure to generate topographical patterns in polymeric materials by a combination of temperature and pressure [46]. SEM and profilometry characterizations of the microchannels fabricated by hot-embossing of PC films show that the geometrical characteristics of the microchannels are in good agreement with the dimensions of the silicon mold used for their fabrication (Fig. 5). This testifies for the robustness of this rapid and easy approach to produce well-defined microchannels.

To functionalize the various PC substrates, we selected the PC-PEI(HA/CHI)$_{12.5}$ LbL architecture, corresponding to a homogeneous film of *ca.* 100 nm dry thickness. The PEI layer is added to improve the anchoring of the LbL film on the PC surface, and the ending HA layer provides an excess of carboxylic acid groups for peptide grafting *via* carbodiimide chemistry. Covalent crosslinking of the LbL film [47] was performed before peptide grafting in order to modify its mechanical properties, thereby presumably increasing its cell-adhesiveness and cell-proliferative properties [48]. The comparison of dry and wet thicknesses of a crosslinked PC-PEI(HA/CHI)$_{12.5}$ film (PC-LbL) shows that such a LbL film swells by a factor of about 60 when immersed in aqueous solution. This high degree of swelling indicates a very soft and open film, compatible with the observed exponential growth of the films (Fig. 2) which was also reported by others [49].

For the next bio-functionalization step, peptides were selected to induce adhesion (RGD) and angiogenesis/tube-like formation (SVV and QK). Our results demonstrate that a FITC-tagged RGD peptide penetrates into the entire swollen LbL film in wet conditions (Fig. 3C). It would therefore be appropriate to report the peptide grafting density per unit volume of film instead as per unit surface of sample. However, as we did not find any reported peptide grafting density per unit volume in the literature, we elicited to also report the peptide grafting density per unit of surface area.

RGD was used to improve cell adhesion, as reported before [50-52]. Previous work demonstrated that a RGD grafting density as low as 1 fmol/mm^2 is enough to improve cell adhesion and spreading on glass surfaces [53]. In other works, using PET [41] or titanium [54] substrates, the grafted RGD density was reported to be 1.8 and 6 pmol/mm^2, respectively. In the more recent work of Gribova *et al.,* the amount of RGD grafted onto/into a LbL made of (polyglycolic acid/poly-L-lysine)$_6$-polyglycolic acid-RGD was evaluated to be 3 pmol/mm^2 [55]. Chua *et al*. successfully grafted RGD on Ti-(HA/CHI)$_5$ bilayers using EDC/NHS chemistry, reporting a density of about

0.145 ± 0.004 pmol/mm^2 [28]. Leslie-Barbick *et al.* successfully immobilized RGD on PEG hydrogels with a peptide density as high as 80 pmol/mm^2 [56]. In the present work, the RGD (GRGDS sequence) grafting density was found to be 18 ± 3 pmol/mm^2 (11 molecules/nm^2). This value lies in-between the one reported by Gribova *et al.* (CGPKGDRGDAGPKGA sequence) [55] and the one reported by Leslie-Barbick *et al.* (RGDS sequence) [56], and is much higher than the minimum RGD density required for cell adhesion reported by Massia *et al.* [53].

Regarding angiogenesis, the SVV peptide was selected since it is a potent angiogenic factor with a similar impact as VEGF in solution, inducing the formation of capillaries [30]. When grafted onto a material surface, SVV was reported to be able to provide both cell adhesion and promote neovascularization in an artificial bone marrow scaffold [25, 31, 57, 58]. SVV was already successfully grafted onto modified gold substrates using EDC/sulfo-NHS chemistry resulting in 1.6 ± 0.2 pmol/mm^2 [59], and on PET surfaces resulting in 20 pmol/mm^2 using the same chemistry [58]. The SVV peptide density measured on our PC-SVV samples is 34 ± 4 pmol/mm^2 (21 molecules/nm^2) which is higher than previously reported values [58] and again points to the probable grafting of SVV throughout the entire film. Therefore we expect that cells will be capable of binding to the immobilized SVV peptide, triggering intracellular signaling for angiogenesis on HUVECs and the formation of tubular-like structures.

QK is another VEGF-mimicking peptide which has already been largely studied for the *in vitro* activation of VEGF receptors (VEGFRs) [34] and for the *in vivo* enhancement of the neovascularization of wounds in mice [60, 61]. After immobilization on a surface, it was shown that QK preserves its bioactive properties in terms of angiogenetic potential. Chan *et al.* have demonstrated a local increase of HUVEC tubulogenesis and an increase of endothelial sprouting on collagen substrates covered with QK at a density of 55 pmol/mm^2 [33]. Leslie-Barbick *et al.* demonstrated that covalently-immobilized QK increases *in vitro* HUVEC migration and tubulogenesis and *in vivo* angiogenesis. In their studies, 23 pmol/mm^2 of QK were immobilized on PEG hydrogels [56]. A peptide density of 55 pmol/mm^2 (33 molecules/nm^2) was measured for PC-QK sample, which is similar to the density achieved by Chan *et al.* [33] and comparable to the one investigated on PEG hydrogels by Leslie-Barbick *et al.* [56]. Therefore, as in the case of SVV, we expect to observe a significant impact of immobilized QK on the development of tubular structures, when grafted onto/into the LbL cushion .

In our studies, cells were seeded in a serum-free medium for 4 h whatever the cell experiments done (XTT test and tubulogenesis assay) or the selected materials. This excludes protein adsorption on the surface during this step [62], which would have contributed to cell adhesion or tubulogenesis, and thus allows us to focus on the specific interaction between the cell receptors and the grafted peptides. HUVECs are largely used for the study of angiogenesis and the formation of vessel-like structures in vascular tissue engineering [63-65]. The studies on their metabolic activity showed a higher metabolism for cells cultured on surfaces grafted with peptide combinations such as RGD+QK and RGD+SVV compared to surfaces grafted with a single peptide. Likewise, it was shown that the co-immobilization of RGD with VEGF [66] or bFGF [67] or insulin leads to a synergistic effect on endothelial cell adhesion and proliferation compared to RGD immobilization only. The cross-talk between the receptor 2 for VEGF and RGD-binding integrins has been investigated before [68-71], highlighting a possible synergistic effect in terms of cellular adhesion, focal adhesion order, integrin activation and migration speed. Le Saux *et al.* reported in a previous work an enhanced endothelial cell response depending on the grafting density of RGD [69]. Noel *et al.* reported a successful grafting of RGD peptide (1 nmol/cm^2) and VEGF protein (50 fmol/cm^2) showing a clear evidence of the additive effect of their combination in terms of HUVECs proliferation, compared to the single RGD or single VEGF condition [66].

Different sources of primary endothelial cells can be used for *in vitro* experiments, such as human dermal microvascular endothelial cells (HDMVECs) [72], human coronary artery endothelial cells (HCAECs) [73], human aortic endothelial cells (HAECs) [74], human pulmonary artery endothelial cells (HPAECs) [75], and human umbilical vein endothelial cells (HUVECs)[25, 57, 58]. Among those variety of primary cells, HUVECs are predominantly used for tissue engineering studies for both large and small vasculature development, since they preserve nearly all the native vascular endothelium features [21, 76]. They have been already investigated within microchannels for transendothelial studies after reaching confluency [77]. In addition, Mori *et al.* developed an interesting system of perfusable channels to supplement a skin-equivalent graft by seeding HUVECs in channels made of collagen and with a width of about 500 µm [78]. Tocchio *et al.* developed a perfusable microchannel system using sacrificial templating and 2-hydroxyethyl methacrylate (HEMA), agarose and gelatin methacrylate (GelMA) seeded with HUVECs [79]. Those studies investigate the formation of microvasculature using large channel sizes of *ca.* 300 µm width, whereas our work focuses on the smallest limit of a capillary vessels, which *in vivo* presents diameters from 10 to 15 µm [18], a size which was so far largely unexplored.

Thanks to the fabrication of microchannels with a proper diameter and surface functionalization combining LbL coating and peptide grafting, we were able to test the formation of capillary tubes by HUVECs depending on surface biochemistry. PC-µCh-RGD+QK and PC-µCh-RGD+SVV materials largely improve the adhesion of HUVECs on the inner sides of microchannels, compared to PC-µCh-LbL samples without peptide. Migration of HUVECs from the side of the channels to the top mesas of the micropatterned surfaces occurs on these peptide-modified samples after 5 h incubation, whereas the formation of tube-like structures starts after 2 h incubation in both cases. Notably, only the PC-RGD+QK material allows to maintain the tube-like structures for longer incubation times, up to 4 h. In the 3D environment of our micro-channel systems, as the formation of tube-like structures is only observed in the presence of at least two HUVECs, the cord hollowing mechanism appears to be more probable than the cell-hollowing mechanism for the lumen formation [24, 25], while in a previously reported study case of 2D patterned material, both mechanisms were involved [25].

The very promising potential of achieving the formation of tubular structures after only 2 h of culture was never reached before, especially in such small microchannels with a diameter of about 25 µm. In the study performed by Mori *et al*, the formation of giant capillaries (with a diameter of about 500 µm) was achieved after 6 days of perfusion [78], while Tocchio *et*

al. proved the formation of smaller capillaries (with a diameter of about 300 µm) after 7 days of perfusion [79]. Due to large differences in size, it is impossible for us to conduct a straightforward comparison between our microchannels of 25 µm and the previously published results on channels 300-500 µm in size. This size difference surely influences the vessel development, as demonstrated by the times at which tube-like structures start to appear: 2 h in our study *versus* 6-7 days in previous works. However, in our study, vessel regression occurred after a few hours, which led us to investigate a supplementary approach to stabilize the tubular structure developed by HUVECs. Regrettably, there is no published information on vessel regression that can be discussed for comparison.

Co-cultures combining HUVECs with various cell lines such as pericytes or mesenchymal stromal stem cells have been already investigated for the stabilization of capillary-like structures formed by HUVECs [58, 80]. Pericytes are perivascular cells which wrap around the endothelium of capillaries, arterioles, venules and also larger vessels [26, 81]. In the field of microvascular tissue engineering, pericytes are largely used because they play an important role in the regulation of capillary diameter, the formation of adherent junctions, the secretion of extracellular matrix proteins, and vessel stabilization *via* release of small molecule release [80]. There is a controversial discussion about the differences and the similarities between mesenchymal stromal stem cells and pericytes. It appears that both cell types share several markers (*e.g.*, CD37, CD90 and CD105). Moreover, they can differentiate in different lineages and play both a role in the stabilization of the endothelium of micro-vascular tissue [81]. However, some *in vitro* experiments showed a stronger impact of pericytes, compared to mesenchymal stromal stem cells, for the stabilization of 50 µm micro-vascular vessels [58].

Therefore, to maintain the tube-like structure formed by HUVECs on the PC-SVV+QK materials after 2 h incubation, co-cultures of HUVECs and hPCs-PL were tested. Analyzed samples show indeed that the presence of hPCs-PL in the microchannels allows to preserve the tube-like structure for longer times, even after 4h incubation. Even though the mechanisms of stabilization are not elucidated in our work, it has been reported that pericytes are capable to stabilize tube-like structure even without a direct cell-cell contact. It was indeed proven that HUVECs and pericytes communicate via the release of several factors such as angiopoietin1 and 2, through the TIE2 receptor [82]. Kim *et al.* developed a co-culture system based on HUVECs and pericytes, in 500 µm microchannels coated with fibrin [27]. After 4 days of co-culture, they observed the formation of vessel-like structures, with the presence of pericytes covering the abluminal surface of the endothelium [27]. Westein *et al.* performed a co-culture microfluidic system in microchannels of 120-500 µm coated with collagen [83]. After 12 h of perfusion, they observed the formation of a single tube-like structure in the presence of the co-culture without TGF-B pathway inhibitor, and no tube-like formation in the presence of the TGF-B inhibitor [84]. This underlines the complexity of capillary stabilization, which does not necessarily works when a supportive cell line, like pericytes, is present. Although these studies used setups which differ strongly from ours, they underline the importance of co-culture systems based on HUVECs and pericytes to form rapidly stable micro-vascular structures, a fact which is also confirmed by our own study.

5. Conclusion

PC microchannels of small width (*ca.* 25 µm) were successfully fabricated by embossing and further functionalized by depositing a polysaccharide (HA/CHI) multilayer film. After crosslinking, this homogeneous coating provides a very efficient anchoring layer for the covalent grafting of RGD, SVV and QK peptides. HUVECs adhesion and metabolic activity were investigated on those samples resulting in improved conditions when a combination of two grafted peptides, either RGD and SVV or RGD and QK, was used. These newly developed bio-functionalized microchannels substrates were further used for tubulogenesis experiments. Formation of tubular structures was observed after just 2 h of incubation for both double-peptide combinations, albeit with a longer stability for the PC-RGD+QK material which is thus the best candidate for mono-culture application in the development of tubular-like structures. Finally, the study in co-culture with hPCs-PL and HUVECs demonstrates that some stabilization of tubular-like structures can be achieved in the PC-PEI(HA/CHI)$_{12.5}$-RGD+SVV material, with a prolongation of their lifetime to up to 4 h after first culture seeding. Altogether, these results prove that our micropatterned platform is a powerful tool to initiate the tubulogenesis from endothelial cells. In the future, this micropatterned platform should be connected to a microfluidic system providing a continuous supply of nutrients and oxygen to achieve the long-time stabilization of the vessels.

Owing to the versatility of LbL assembly, and to the very simple molding technique used to create microchannels, our approach might be easily transferred to other biomaterials while preserving the angiogenic properties. The potential applications of the rapid development of small micro-vascular structures can be wide, considering that the majority of organs and tissues require a functional micro-vasculature to be efficiently perfused with oxygen and nutrients. This innovative approach for real capillary-size tube-like formation in an extremely short time represents a simple model for the production of capillaries made of HUVECs and stabilized with hPCs-PL, which could be used for studying inhibitors and activators of angiogenesis and thereby present opportunities to progress further in the field of tissue engineering. Moreover, to improve the efficacy of our model, further studies investigating the influence of the microchannels diameter on the tubular formation would be of interest.

ACKNOWLEDGMENT

The authors thank Colette Douchamps, Cécile D'Haese and Delphine Magnin for technical assistance at UCLouvain. They also thank Sébastien Marais, and Christel Poujol from BIC imaging center for their help with the CLSM. it4ip company is thanked for having provided the polycarbonate films. This work was performed as a part of the EJD-FunMat project, founded by the European Union's Horizon 2020 research and innovation program, under the Marie Sklodowska-Curie grant agreement No. 641640. K. G. is Research Associate of the F. R. S.–FNRS.

REFERENCES

1. Lokmic Z and Mitchell GM. *Engineering the microcirculation*. Tissue Eng Part B 2008; **14**(1): 87-103.

2. Zhang B, Montgomery M, Chamberlain MD, Ogawa S, Korolj A, Pahnke A, Wells LA, Massé S, Kim J, and Reis L. *Biodegradable scaffold with built-in vasculature for organ-on-a-chip engineering and direct surgical anastomosis*. Nat Materials 2016; **15**(6): 669.
3. Kim S, Chung M, Ahn J, Lee S, and Jeon NL. *Interstitial flow regulates the angiogenic response and phenotype of endothelial cells in a 3D culture model*. Lab on a Chip 2016; **16**(21): 4189-4199.
4. Frerich B, Lindemann N, Kurtz-Hoffmann J, and Oertel K. *In vitro model of a vascular stroma for the engineering of vascularized tissues*. Int J Oral & Maxioll Surgery 2001; **30**(5): 414-420.
5. Atala A, Kasper FK, and Mikos AG. *Engineering complex tissues*. Sci Transl Med 2012; **4**(160): 160rv112-160rv112.
6. Cheng F, Cao X, Li H, Liu T, Xie X, Huang D, Maharjan S, Bei HP, Gómez A, and Li J. *Generation of Cost-Effective Paper-Based Tissue Models through Matrix-Assisted Sacrificial 3D Printing*. Nano letters 2019.
7. Laschke MW and Menger MD. *Prevascularization in tissue engineering: current concepts and future directions*. Biotechnol Adv 2016; **34**(2): 112-121.
8. Rouwkema J and Khademhosseini A. *Vascularization and angiogenesis in tissue engineering: beyond creating static networks*. Trends Biotechnol 2016; **34**(9): 733-745.
9. Song H-HG, Rumma RT, Ozaki CK, Edelman ER, and Chen CS. *Vascular tissue engineering: progress, challenges, and clinical promise*. Cell stem cell 2018; **22**(3): 340-354.
10. Unger RE, Dohle E, and Kirkpatrick CJ. *Improving vascularization of engineered bone through the generation of pro-angiogenic effects in co-culture systems*. Adv Drug Del Rev 2015; **94**: 116-125.
11. Barabaschi GD, Manoharan V, Li Q, and Bertassoni LE, *Engineering pre-vascularized scaffolds for bone regeneration*, in *Engineering Mineralized and Load Bearing Tissues*. 2015, Springer. p. 79-94.
12. Brockport CA, College CC, CC CBoM, College CBC, College CHC, College FMC, College GC, College HCC, College MC, Textbooks OS, College P, ESF S, Technology SFIo, Fredonia S, Oswego S, Potsdam S, and Albany UA, *Anatomy and Physiology II*, Oe access, Editor., Lumen learning: Lumen learning.
13. J. Gordon Betts TJC, Dean H. Kruse PCC, Kelly A. Young CSU, Long Beach, Brandon Poe STCC, Peter DeSaix UoNCaCH, Oksana Korol ACC, James A. Wise HU, Eddie Johnson COCC, Jody E. Johnson ACC, Mark Womble YSU, William Blaker FU, Julie Bowers ETSU, Matthew Barlow ENMU, Michael Hortsch UoM, Emily Bradshaw FSC, Nishi Bryska UoNC, Charlotte, Susan Caley Opsal IVCC, Kathleen Tallman APU, Boyd Campbell SCoNMaHS, Rohinton Tarapore UoP, Branko Jablanovic CoLC, Pamela Dobbins SSCC, Norman Johnson UoMA, Kenneth Crane TC, Barbara Christie-Pope CC, Douglas Sizemore BSCC, Maurice Culver FSCaJ, Debra McLaughlin UoMUC, Bruce Maring DSC, David Wortham WGTC, Heather Cushman TCC, Elizabeth DuPriest WPC, Peter Dukehart TRCC, Susan Dentel WCC, Elizabeth Tattersall WNC, Susanna Heinze SVC, Julie May WCU, Ann Caplea WU, Timothy Ballard UoNCW, Phillip Nicotera SPC, Marnie Chapman UoA, Sitka, William Kleinelp MCC, Brenda Leady UoT, Sarah Leupen UoM, Baltimore County, Robert Mallet UoNTHSC, Michael Giangrande OCC, Natalie Maxwell CASC, Sallisaw, Lynn Gargan TCC, Mark Jonasson NAC, Leigh Kleinert GRCC, Dale Horeth TCC, Kathleen Weiss GFU, Betsy Ott TJC, Sharon Ellerton QCC, Janis Thompson LCCC, Rita Thrasher PSC, Nicholas Mitchell SBU, David Van Wylen SOC, Elisabeth Martin CoLC, Ivan Paul JWCC, Lihua Liang JHU, Sondra Dubowsky MCC, Mary Jane Niles UoSF, Mark Thomas UoNC, Mike Pyle ONU, Thomas

Pilat ICC, Ikemefuna Nwosu PCLLC, Patty Dolan PLU, Ellen DuPré CC, John Lepri UoNC, Greensboro, Carla Endres USU-CoEUSJC, Ann Henninger WC, Susan Spencer MHCC, Rosemary Hubbard MU, Aaron Payette CoSN, Greg Fitch AU, Robert Sullivan MC, AnnMarie DelliPizzi DC, Cynthia Standley UoA, Shobhana Natarajan BC, Scott Payne KWC, Laird Sheldahl MHCC, Jason Schreer SUoNYaP, Pam Elf UoM, Umesh Yadav UoTMB, Cameron Perkins SGC, Robert Rawding GU, Brian Shmaefsky LSCS, Chaya Gopalan SLCoP, Mark Hubley PGsCC, Jeff Keyte CoSM, Victor Greco CTC, Robert Allison MCC, Heather Armbruster SUSCC, Lynn Wandrey MCC, David Pfeiffer UoA, Anchorage, Eileen Preston TCC, Eric Sun MGSC, Tom Swenson IC, Tony Yates OBU, Justin York GCC, Cheri Zao NIC, Elena Zoubina BSUMCC, Noelle Cutter MC, Lynnette Danzl-Tauer RVC, Myriam Feldman LWIoTCCC, Margaret Weck SLCoP, Neil Westergaard WSC, Jane Davis AU, Kim Aaronson AITC, Lopamudra Agarwal ATC, Gary Allen DU and Shobhana Natarajan AL, Inc, *Anatomy and Physiology*, ed. OpenStax. 2013.

14. Kim JJ, Hou L, and Huang NF. *Vascularization of three-dimensional engineered tissues for regenerative medicine applications*. Acta Biomater 2016; **41**: 17-26.
15. Raghavan S, Nelson CM, Baranski JD, Lim E, and Chen CS. *Geometrically controlled endothelial tubulogenesis in micropatterned gels*. Tissue Eng Part A 2010; **16**(7): 2255-2263.
16. Sivarapatna A, Ghaedi M, Xiao Y, Han E, Aryal B, Zhou J, Fernandez-Hernando C, Qyang Y, Hirschi KK, and Niklason LE. *Engineered Microvasculature in PDMS Networks Using Endothelial Cells Derived from Human Induced Pluripotent Stem Cells*. Cell Transpl 2017; **26**(8): 1365-1379.
17. Tsvirkun D, Grichine A, Duperray A, Misbah C, and Bureau L. *Microvasculature on a chip: study of the Endothelial Surface Layer and the flow structure of Red Blood Cells*. Sci Rep 2017; **7**: 45036.
18. Kannan RY, Salacinski HJ, Sales K, Butler P, and Seifalian AM. *The roles of tissue engineering and vascularisation in the development of micro-vascular networks: a review*. Biomaterials 2005; **26**(14): 1857-1875.
19. Warren B, Shubik P, Wilson R, Garcia H, and Feldman R. *The microcirculation in two transplantable melanomas of the hamster II. Scanning electron microscopy*. Cancer Lett 1978; **4**: 117-124.
20. Monticone G, Colonna L, Palermi G, Bono R, and Puddu P. *Quantitative nailfold capillary microscopy findings in patients with acrocyanosis compared with patients having systemic sclerosis and control subjects*. Journal of the American Academy of Dermatology 2000; **42**(5): 787-790.
21. Perry L, Ben-Shaul S, Landau S, and Levenberg S. *Co-culture systems for vasculogenesis*. Vasc Tissue Eng Reg Med 2017: 1-29.
22. Gilbert-Honick J, Iyer SR, Somers SM, Lovering RM, Wagner K, Mao H-Q, and Grayson WL. *Engineering functional and histological regeneration of vascularized skeletal muscle*. Biomaterials 2018; **164**: 70-79.
23. Sasaki K, Akagi T, Asaoka T, Eguchi H, Fukuda Y, Iwagami Y, Yamada D, Noda T, Wada H, and Gotoh K. *Construction of three-dimensional vascularized functional human liver tissue using a layer-by-layer cell coating technique*. Biomaterials 2017; **133**: 263-274.
24. Iruela-Arispe ML and Davis GE. *Cellular and molecular mechanisms of vascular lumen formation*. Dev Cell 2009; **16**(2): 222-231.
25. Lei Y, Zouani OF, Rémy M, Ayela C, and Durrieu M-C. *Geometrical microfeature cues for directing tubulogenesis of endothelial cells*. PloS one 2012; **7**(7): e41163.
26. Andreeva E, Pugach I, Gordon D, and Orekhov A. *Continuous subendothelial*

network formed by pericyte-like cells in human vascular bed. Tissue and Cell 1998; **30**(1): 127-135.

27. Kim S, Lee H, Chung M, and Jeon NL. *Engineering of functional, perfusable 3D microvascular networks on a chip*. Lab on a Chip 2013; **13**(8): 1489-1500.
28. Chua P-H, Neoh K-G, Kang E-T, and Wang W. *Surface functionalization of titanium with hyaluronic acid/chitosan polyelectrolyte multilayers and RGD for promoting osteoblast functions and inhibiting bacterial adhesion*. Biomaterials 2008; **29**(10): 1412-1421.
29. Hersel U, Dahmen C, and Kessler H. *RGD modified polymers: biomaterials for stimulated cell adhesion and beyond*. Biomaterials 2003; **24**(24): 4385-4415.
30. Hamada Y, Nokihara K, Okazaki M, Fujitani W, Matsumoto T, Matsuo M, Umakoshi Y, Takahashi J, and Matsuura N. *Angiogenic activity of osteopontin-derived peptide SVVYGLR*. Biochem Biophys Res Commun 2003; **310**(1): 153-157.
31. Hamada Y, Egusa H, Kaneda Y, Hirata I, Kawaguchi N, Hirao T, Matsumoto T, Yao M, Daito K, and Suzuki M. *Synthetic osteopontin-derived peptide SVVYGLR can induce neovascularization in artificial bone marrow scaffold biomaterials*. Dental Mat J 2007; **26**(4): 487-492.
32. D'Andrea LD, Iaccarino G, Fattorusso R, Sorriento D, Carannante C, Capasso D, Trimarco B, and Pedone C. *Targeting angiogenesis: structural characterization and biological properties of a de novo engineered VEGF mimicking peptide*. Proceedings of the National Academy of Sciences 2005; **102**(40): 14215-14220.
33. Chan TR, Stahl PJ, and Yu SM. *Matrix-Bound VEGF Mimetic Peptides: Design and Endothelial-Cell Activation in Collagen Scaffolds*. Adv Funct Mat 2011; **21**(22): 4252-4262.
34. Di Stasi R, Diana D, Capasso D, Di Gaetano S, De Rosa L, Celentano V, Isernia C, Fattorusso R, and D'Andrea LD. *VEGFR recognition interface of a proangiogenic VEGF-mimetic peptide as determined in vitro and in presence of endothelial cells by NMR spectroscopy*. Chem Europ J 2018.
35. Pallandre A, Glinel K, Jonas AM, and Nysten B. *Binary nanopatterned surfaces prepared from silane monolayers*. Nano Letters 2004; **4**(2): 365-371.
36. Feng Q, Zeng G, Yang P, Wang C, and Cai J. *Self-assembly and characterization of polyelectrolyte complex films of hyaluronic acid/chitosan*. Colloids and Surfaces A: Physicochemical and Engineering Aspects 2005; **257**: 85-88.
37. Croll TI, O'Connor AJ, Stevens GW, and Cooper-White JJ. *A blank slate? Layer-by-layer deposition of hyaluronic acid and chitosan onto various surfaces*. Biomacromolecules 2006; **7**(5): 1610-1622.
38. Croisier F, Atanasova G, Poumay Y, and Jérôme C. *Polysaccharide-Coated PCL Nanofibers for Wound Dressing Applications*. Adv Healthcare Mat 2014; **3**(12): 2032-2039.
39. Li H, Ge Y, Zhang P, Wu L, and Chen S. *The effect of layer-by-layer chitosan–hyaluronic acid coating on graft-to-bone healing of a poly (ethylene terephthalate) artificial ligament*. Journal of Biomaterials Science, Polymer Edition 2012; **23**(1-4): 425-438.
40. Chollet C, Chanseau C, Brouillaud B, and Durrieu M. *RGD peptides grafting onto poly (ethylene terephthalate) with well controlled densities*. Biomol Eng 2007; **24**(5): 477-482.
41. Chollet C, Chanseau C, Remy M, Guignandon A, Bareille R, Labrugère C, Bordenave L, and Durrieu M-C. *The effect of RGD density on osteoblast and endothelial cell behavior on RGD-grafted polyethylene terephthalate surfaces*. Biomaterials 2009; **30**(5): 711-720.
42. Uchida E, Uyama Y, and Ikada Y. *Surface graft polymerization of ionic monomers onto poly (ethylene terephthalate) by UV-irradiation without degassing*. J Appl Polym Sci 1993; **47**(3): 417-424.

43. Coufal NG, Garcia-Perez JL, Peng GE, Yeo GW, Mu Y, Lovci MT, Morell M, O'Shea KS, Moran JV, and Gage FH. *L1 retrotransposition in human neural progenitor cells*. Nature 2009; **460**(7259): 1127.
44. Kujawa P, Moraille P, Sanchez J, Badia A, and Winnik FM. *Effect of molecular weight on the exponential growth and morphology of hyaluronan/chitosan multilayers: A surface plasmon resonance spectroscopy and atomic force microscopy investigation*. J Am Chem Soc 2005; **127**(25): 9224-9234.
45. Monge C, Almodóvar J, Boudou T, and Picart C. *Spatio-temporal control of LbL films for biomedical applications: from 2D to 3D*. Adv Healthcare Mat 2015; **4**(6): 811-830.
46. Debono M, Voicu D, Pousti M, Safdar M, Young R, Kumacheva E, and Greener J. *One-step fabrication of microchannels with integrated three dimensional features by hot intrusion embossing*. Sensors 2016; **16**(12): 2023.
47. Picart C. *Polyelectrolyte multilayer films: from physico-chemical properties to the control of cellular processes*. Curr Med Chem 2008; **15**(7): 685-697.
48. Schneider A, Francius G, Obeid R, Schwinté P, Hemmerlé J, Frisch B, Schaaf P, Voegel J-C, Senger B, and Picart C. *Polyelectrolyte multilayers with a tunable Young's modulus: influence of film stiffness on cell adhesion*. Langmuir 2006; **22**(3): 1193-1200.
49. Richert L, Lavalle P, Payan E, Shu XZ, Prestwich GD, Stoltz J-F, Schaaf P, Voegel J-C, and Picart C. *Layer by layer buildup of polysaccharide films: physical chemistry and cellular adhesion aspects*. Langmuir 2004; **20**(2): 448-458.
50. Wang Z, Dong L, Han L, Wang K, Lu X, Fang L, Qu S, and Chan CW. *Self-assembled Biodegradable Nanoparticles and Polysaccharides as Biomimetic ECM Nanostructures for the Synergistic effect of RGD and BMP-2 on Bone Formation*. Sci Rep 2016; **6**: 25090.
51. Kapp TG, Rechenmacher F, Neubauer S, Maltsev OV, Cavalcanti-Adam EA, Zarka R, Reuning U, Notni J, Wester H-J, and Mas-Moruno C. *A comprehensive evaluation of the activity and selectivity profile of ligands for RGD-binding integrins*. Sci Rep 2017; **7**: 39805.
52. Anjum F, Agabalyan NA, Sparks HD, Rosin NL, Kallos MS, and Biernaskie J. *Biocomposite nanofiber matrices to support ECM remodeling by human dermal progenitors and enhanced wound closure*. Sci Rep 2017; **7**(1): 10291.
53. Massia SP and Hubbell JA. *An RGD spacing of 440 nm is sufficient for integrin alpha V beta 3-mediated fibroblast spreading and 140 nm for focal contact and stress fiber formation*. J cell biol 1991; **114**(5): 1089-1100.
54. Porté-Durrieu M-C, Guillemot F, Pallu S, Labrugère C, Brouillaud B, Bareille R, Amédée J, Barthe N, Dard M, and Baquey C. *Cyclo-(DfKRG) peptide grafting onto Ti–6Al–4V: physical characterization and interest towards human osteoprogenitor cells adhesion*. Biomaterials 2004; **25**(19): 4837-4846.
55. Gribova V, Gauthier-Rouvière C, Albigès-Rizo C, Auzely-Velty R, and Picart C. *Effect of RGD functionalization and stiffness modulation of polyelectrolyte multilayer films on muscle cell differentiation*. Acta Biomater 2013; **9**(5): 6468-6480.
56. Leslie-Barbick JE, Saik JE, Gould DJ, Dickinson ME, and West JL. *The promotion of microvasculature formation in poly (ethylene glycol) diacrylate hydrogels by an immobilized VEGF-mimetic peptide*. Biomaterials 2011; **32**(25): 5782-5789.
57. Lei Y, Rémy M, Labrugère C, and Durrieu M-C. *Peptide immobilization on polyethylene terephthalate surfaces to study specific endothelial cell adhesion, spreading and migration*. Journal of Materials Science: Materials in Medicine 2012; **23**(11): 2761-2772.

58. Zouani OF, Lei Y, and Durrieu MC. *Pericytes, Stem-Cell-Like Cells, but not Mesenchymal Stem Cells are Recruited to Support Microvascular Tube Stabilization*. Small 2013; **9**(18): 3070-3075.
59. Le Saux G, Plawinski L, Parrot C, Nlate S, Servant L, Teichmann M, Buffeteau T, and Durrieu MC. *Surface bound VEGF mimicking peptide maintains endothelial cell proliferation in the absence of soluble VEGF in vitro*. Journal of Biomedical Materials Research Part A 2016; **104**(6): 1425-1436.
60. Fu J and Wang D-A. *In Situ Organ-Specific Vascularization in Tissue Engineering*. Trends Biotechnol 2018.
61. Santulli G, Ciccarelli M, Palumbo G, Campanile A, Galasso G, Ziaco B, Altobelli GG, Cimini V, Piscione F, and D'Andrea LD. *In vivo properties of the proangiogenic peptide QK*. J Transl Med 2009; **7**(1): 41.
62. Yang D, Lü X, Hong Y, Xi T, and Zhang D. *The molecular mechanism of mediation of adsorbed serum proteins to endothelial cells adhesion and growth on biomaterials*. Biomaterials 2013; **34**(23): 5747-5758.
63. Suntornnond R, Tan EYS, An J, and Chua CK. *A highly printable and biocompatible hydrogel composite for direct printing of soft and perfusable vasculature-like structures*. Sci Rep 2017; **7**(1): 16902.
64. Datta P, Ayan B, and Ozbolat IT. *Bioprinting for vascular and vascularized tissue biofabrication*. Acta Biomater 2017; **51**: 1-20.
65. Ma Y-HV, Middleton K, You L, and Sun Y. *A review of microfluidic approaches for investigating cancer extravasation during metastasis*. Microsystems & Nanoeng 2018; **4**: 17104.
66. Noel S, Fortier C, Murschel F, Belzil A, Gaudet G, Jolicoeur M, and De Crescenzo G. *Co-immobilization of adhesive peptides and VEGF within a dextran-based coating for vascular applications*. Acta Biomater 2016; **37**: 69-82.
67. Lee YB, Shin YM, Lee J-h, Jun I, Kang JK, Park J-C, and Shin H. *Polydopamine-mediated immobilization of multiple bioactive molecules for the development of functional vascular graft materials*. Biomaterials 2012; **33**(33): 8343-8352.
68. Eliceiri BP. *Integrin and growth factor receptor crosstalk*. Circul Res 2001; **89**(12): 1104-1110.
69. Le Saux G, Magenau A, Gunaratnam K, Kilian KA, Böcking T, Gooding JJ, and Gaus K. *Spacing of integrin ligands influences signal transduction in endothelial cells*. Biophys J 2011; **101**(4): 764-773.
70. Byzova TV, Goldman CK, Pampori N, Thomas KA, Bett A, Shattil SJ, and Plow EF. *A mechanism for modulation of cellular responses to VEGF: activation of the integrins*. Mol Cell 2000; **6**(4): 851-860.
71. Traub S, Morgner J, Martino MM, Höning S, Swartz MA, Wickström SA, Hubbell JA, and Eming SA. *The promotion of endothelial cell attachment and spreading using FNIII10 fused to VEGF-A165*. Biomaterials 2013; **34**(24): 5958-5968.
72. Borges J, Mueller MC, Padron NT, Tegtmeier F, Lang E, and Stark GB. *Engineered adipose tissue supplied by functional microvessels*. Tissue Eng 2003; **9**(6): 1263-1270.
73. Carter W, Sekharem M, and Hoying J. *56: In vitro generation of human microvessel networks*. J Surg Res 2007; **137**(2): 174.
74. Sfriso R, Zhang S, Bichsel CA, Steck O, Despont A, Guenat OT, and Rieben R. *3D artificial round section micro-vessels to investigate endothelial cells under physiological flow conditions*. Sci Rep 2018; **8**(1): 5898.
75. Hauser S, Jung F, and Pietzsch J. *Human endothelial cell models in biomaterial research*. Trends Biotechnol 2017; **35**(3): 265-277.
76. Park H-J, Zhang Y, Georgescu SP, Johnson KL, Kong D, and Galper JB. *Human umbilical vein endothelial cells and human dermal microvascular endothelial cells offer new insights into the*

relationship between lipid metabolism and angiogenesis. Stem Cell Rev 2006; **2**(2): 93-101.

77. Hebeiss I, Truckenmüller R, Giselbrecht S, and Schepers U. *Novel three-dimensional Boyden chamber system for studying transendothelial transport*. Lab on a Chip 2012; **12**(4): 829-834.
78. Mori N, Morimoto Y, and Takeuchi S. *Skin integrated with perfusable vascular channels on a chip*. Biomaterials 2017; **116**: 48-56.
79. Tocchio A, Tamplenizza M, Martello F, Gerges I, Rossi E, Argentiere S, Rodighiero S, Zhao W, Milani P, and Lenardi C. *Versatile fabrication of vascularizable scaffolds for large tissue engineering in bioreactor*. Biomaterials 2015; **45**: 124-131.
80. Kim J, Chung M, Kim S, Jo DH, Kim JH, and Jeon NL. *Engineering of a biomimetic pericyte-covered 3D microvascular network*. PloS one 2015; **10**(7): e0133880.
81. Crisan M, Yap S, Casteilla L, Chen C-W, Corselli M, Park TS, Andriolo G, Sun B, Zheng B, and Zhang L. *A perivascular origin for mesenchymal stem cells in multiple human organs*. Cell stem cell 2008; **3**(3): 301-313.
82. Teichert M, Milde L, Holm A, Stanicek L, Gengenbacher N, Savant S, Ruckdeschel T, Hasanov Z, Srivastava K, and Hu J. *Pericyte-expressed Tie2 controls angiogenesis and vessel maturation*. Nat Comm 2017; **8**: 16106.
83. Westein E, van der Meer AD, Kuijpers MJ, Frimat J-P, van den Berg A, and Heemskerk JW. *Atherosclerotic geometries exacerbate pathological thrombus formation poststenosis in a von Willebrand factor-dependent manner*. Proceedings of the National Academy of Sciences 2013; **110**(4): 1357-1362.
84. van der Meer AD, Orlova VV, ten Dijke P, van den Berg A, and Mummery CL. *Three-dimensional co-cultures of human endothelial cells and embryonic stem cell-derived pericytes inside a microfluidic device*. Lab on a Chip 2013; **13**(18): 3562-3568.